LONG PERIOD GRATING FIBER TEMPERATURE SENSOR EMBEDDED INTO POLYMER MATRIX OF AN AUTOMOBILE COMPOSITE MATERIAL MECHANICAL PART

Sorin MICLOS[1], Dan SAVASTRU[2], Roxana SAVASTRU[3], Florina-Gianina ELFARRA[4], and Ion LANCRANJAN[5]

The reinforced polymer composites service life depends on long term aggressive environments. Among the ageing environment mechanism an important one is the combination of moderate high temperature and moisture. Long Period Grating Fiber Sensors (LPGFS) can be used as sensors embedded into composite material polymer matrix for measuring the moderate high temperature and moisture. There are presented the simulation results of a such LPGFS optical sensor.

Keywords: LPGFS sensor, temperature sensor, smart polymer composite material.

1. Introduction

Presently, in the aerospace and in the automotive industries more and more mechanical parts are made of polymer composite materials. Interest in polymer composite materials is increasing gradually due to the opportunities they present for various applications are necessary their high specific stiffness and strength, weight reduction, fatigue performance, improved thermal and electrical conductivity and the possibility to integrate sensors or actuators [1-10]. Composite material has a complex composition on which depend its final properties correlated on the properties of component materials (polymer matrices, reinforcements, fillers and additives). The design of composite materials is affected by a combination of parameters, including the number of layers, the

[1] Eng., National Institute of R&D for Optoelectronics- INOE 2000, Romania, e-mail: miclos@inoe.ro
[2] Dr. Eng., National Institute of R&D for Optoelectronics- INOE 2000, Romania, e-mail: dsavas@inoe.ro
[3] Dr. Eng., National Institute of R&D for Optoelectronics- INOE 2000, Romania, e-mail: rsavas@inoe.ro
[4] Phys., "Saint John" Emergency Clinical Hospital e-mail: gianina.elfarra@gmail.com
[5] Phys., National Institute of R&D for Optoelectronics- INOE 2000, Romania, e-mail: ion.lancranjan@inoe.ro

material combinations, ply directions and manufacturing method. Composite materials can be manufactured using a variety of methods available nowadays, such as vacuum, autoclave, Resin Transfer Molding (RTM) and Liquid Resin Infusion (LRI) [1-10].

Structural Health Monitoring (SHM) concept aims to give, at every moment during the life of a structure, a diagnosis of the status of the constituent materials, of the different parts, and of the full assembly of these parts constituting the structure as a whole with the purpose of most efficient use of advanced composites in aerospace and automotive fields [1-10]. Also, SHM represents the use of in-situ, non-destructive sensing and analysis of structural characteristics, including the structural response, for detecting changes that may indicate damage or degradation [8-10]. Nevertheless, an important parameter to be watched in the SHM frame is the temperature of the polymer composite materials [1-10].

Composite materials damage, health and structural monitoring are described by proposed many definitions. Structure health is defined as the ability to function and maintain the structural integrity during the entire life of a structure. Damage is defined as a material, structural or functional failure, or as a change in physical parameters, such as mass, stiffness or damping. Monitoring is the process of structural diagnosis and prognosis [1-10]. SHM is considered as the observation of a system over time based on periodically sampled response measurements from a sensor network, the extraction of features sensitive to damage and the analysis of these features, in order the system's structural condition - health to be defined [1-10]. It is a very important tool for the current and future design, analysis and maintenance of engineering structures [8]. Temperature is an important composite parameter concerning applications with highly loaded parts, areas susceptible to corrosion and in applications with high fatigue loads [22]. The SHM is strongly correlated with the concept of defects induced in the investigated composite materials, being a measure of detecting defects which are induced into the composite materials such as voids, delamination of polymer matrix and of composite material [1-10]. Temperature is important in the sense that if being increased but kept at values lower than the polymer melting point it has an action in favor of water molecules infiltration into polymer matrix.

2. Theory

Like the commonly used Fiber Bragg Grating (FBG), Long Period Grating (LPG) is sensitive to of the surrounding environment temperature changes [3-10]. Although this property can be exploited advantageously in LPG-based temperature sensors, more often than not it is an undesirable attribute whose effects need to be eliminated (whether this is for thermal stability required in

telecommunications applications, or for LPG-based sensors in which thermal effects could disrupt the detection of another parameter) [3-10]. It is therefore important to fully characterize the variations in LPG transmission spectra (namely shifts in attenuation band central wavelengths, possibly accompanied by peak intensity changes) that are brought about by temperature fluctuations, so that these effects can be controlled or disregarded as necessary. In Fig. 1 there is schematically presented the investigated LPGFS and its operation as a temperature sensor [3-10].

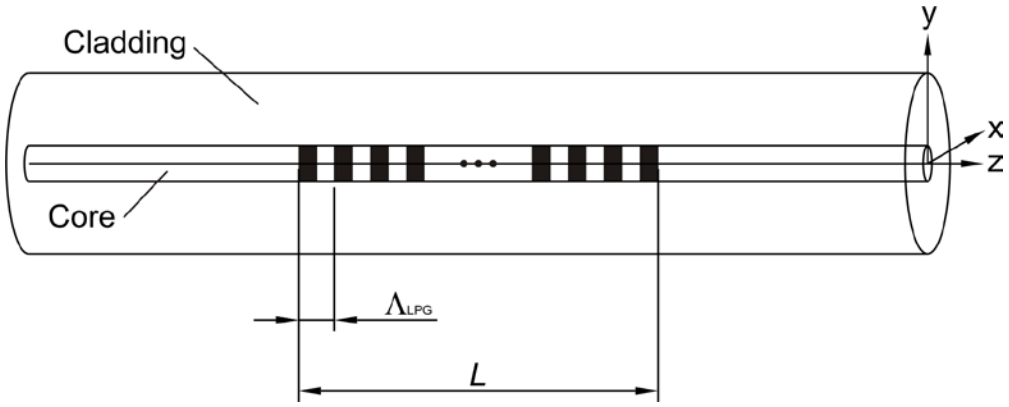

Fig. 1. Schematic representation of a LPGFS.

LPGFS are manufactured into single mode (SM) optical fibers by inducing a permanent modulation of its characteristics (geometrical shape or refractive index). The temperature changes effects on LPGFS can be of two categories. The first category includes effects on optical fiber, namely the thermal expansion or contraction and the thermal optical effect. The former effect occurs in almost all materials and is described as

$$\Delta L = \alpha L \Delta T \tag{1}$$

where L is the length of fiber being observed, and α is called the thermal expansion coefficient, defined for fused silica fibers as $\alpha = 0.55 \cdot 10^{-6}\ ^{o}C^{-1}$ [1, 2]. The second is the effect of temperature on the fiber effective index, described as

$$\Delta n_{eff} = \xi n_{eff} \Delta T \tag{2}$$

which is due mainly to the thermal optic effect of silica material, defined as $dn/dT \sim 1 \cdot 10^{-5}\ K^{-1}$ which is a negligible effect on the waveguide operation of the optical fiber [1,2]. The overall coefficient ξ is about $7 \cdot 10^{-6}\ K^{-1}$, which is one order larger than the thermal expansion effect. Thus, the phase defined as

$$\phi = n_{eff} kL \tag{3}$$

will be modulated by temperature change as

$$\Delta\phi = (\alpha + \xi) n_{eff} kL\Delta T \tag{4}$$

The temperature modulation of light phase leads to

$$\frac{d\lambda^{(m)}}{dT} = \Lambda\left(\frac{dn_{effco}}{dT} - \frac{dn_{effcl}^{(m)}}{dT}\right) + \left(n_{effco} - n_{effcl}^{(m)}\right)\frac{d\Lambda}{dT} \tag{5}$$

where n_{effco} and $n_{effcl}^{(m)}$ are effective values of refractive index of the core and m^{th} cladding propagation mode and Λ is the grating period. Temperature variation will also bring about thermal stress, which comes from the different thermal expansion coefficients between fiber and its packaging structures, including its jackets and protective materials in cabling, and intentionally designed mount structures for fiber sensors. Such thermal stresses have to be analyzed individually for different situations. In practice, temporal variation of temperature and related thermal conduction phenomena induce the dynamic thermal effect, usually in low speed, and cause drifts of signal, which must be dealt seriously, especially for high-precision and high-stability sensors. The LPGFS operation is quite simple. The input light beam having an input spectrum and propagating guided through the core as the fundamental mode is blazing incident on the LPG being diffracted. An LPG acts as an optical fiber-based grating that enables coupling between the core and the cladding co-propagation modes. This coupling between propagation modes represents an electromagnetic energy transfer from the core mode to the possible cladding modes [15-23]. The transferred energy is lost from the fundamental light mode and can continue its propagation through the cladding until it is lost into the ambient, kept into core proximity volume or coupled back, when meeting another LPG, to the fundamental mode. This energy transfer has maximum values at discrete wavelengths λ^i defined by the relation [11-19]

$$\lambda^i = \left(n_{eff} - n_{clad}^i\right) \cdot \Lambda \tag{6}$$

where λ^i is the central wavelength of the attenuation band, n_{eff} is the effective value of the core refractive index, represents the effective value of refractive index of the i^{th} possible cladding propagation mode and Λ is the period of the LPG. Eq. (3) is useful for sensing observing that the effective values of refractive index of core and cladding propagation modes depend on the ambient refractive index [11-17]. Practically any infinitesimal modification of the light propagation through the LPGFS is sensed by the LPG and can be observed by the spectral shifting and broadening of each absorption bands existing in SM optical fiber [11-23]. In the FBG case because the mode coupling caused by the grating between light propagation modes take place only between the fundamental mode and counter-propagating ones, a fact imposed by energy and impulse conservation laws, the single modification of the light spectrum will consist of one sharp reflection band centered at λ_B, the Bragg wavelength [11-23].

3. Simulation results

The simulation results were accomplished considering that the LPGFS is manufactured into a SM optical fiber considered as standard, namely Fibercore SM750 type optical fiber, which is, according to literature, commonly used as host for LPGFS [11-17]. For short, this means that the optical fiber core has a diameter of 2.8 up to 3.5 μm and a refractive index of 1.4585, its cladding has a 62.5 μm diameter with a refractive index of 1.4540 [11-17]. The LPGFS was considered as having a length in the range 5 - 70 mm and a grating period in the range 5 – 500 μm. The simulations were performed considering the optical fiber as embedded in Polycarbonate (PC, i.e. $(C_{16}H_{14}O_3)_n$) matrix of a composite material.

The first step in performing the FBG or LPGFS simulations consists in defining the effective value of SM optical fiber refractive index in Eqs. (1) and (3). In Figs. 2 and 3 there are presented the results obtained in calculation of effective value of core refractive index (n_{effco}) and normalized frequency variation (V_{co}) vs the wavelength λ.

In the LPGFS case there are presented the results obtained in simulating the variations of effective values cladding refractive index with wavelength of the light propagating through the optical fiber core incident on the LPG. n_{clad}^{i} was calculated for the first ten cladding propagation modes.

Then the phase matching curves for the investigated LPGFS are calculated using Eq. (3). The key of LPGFS operation modes becomes clear after analyzing the significance of the phase matching curves. It can be observed that phase matching curves are parametric curves defined into domains of LPG grating period, Λ_{LPG}, and guided light wavelength. The following procedure is quite simple: imagine a horizontal or vertical line, i.e. corresponding to a given value of Λ_{LPG} or light wavelength; the intersection points of this horizontal or vertical line with the phase matching curves defines the peaks λ^i of absorption bands appearing the optic fiber transmission spectrum. In common cases, for a given Λ_{LPG}, at a wavelength of the emission spectrum of a light source coupled to the LPGFS, corresponds several absorption bands each of them being induced by energy transfer to a cladding propagation mode.

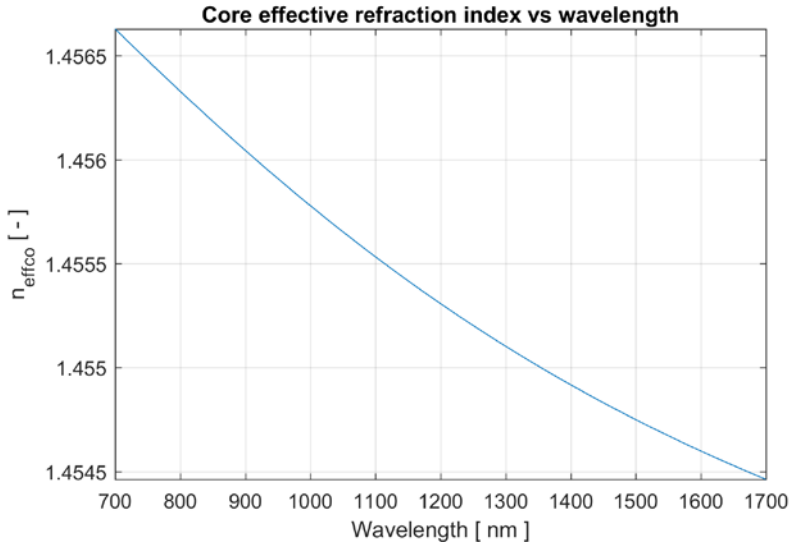

Fig. 2. Simulated variation of core refractive index effective value vs incident light wavelength.

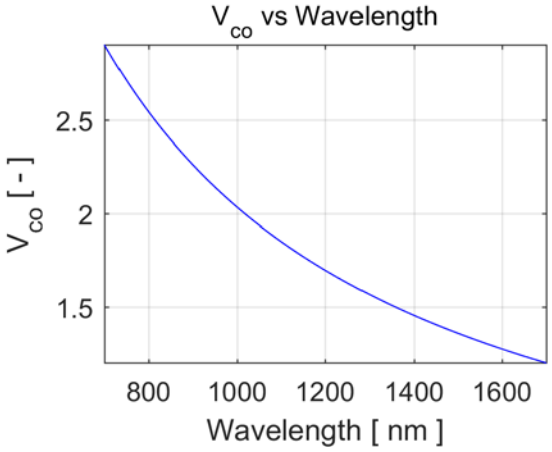

Fig. 3. Simulated variation of core refractive index effective value vs incident light wavelength.

In Fig. 4 there are presented the variations of effective values of refractive index corresponding to the first ten cladding propagation modes simulated for the investigated LPGFS.

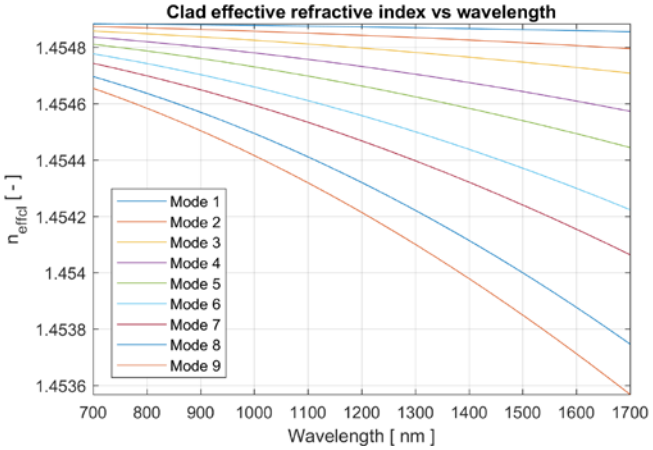

Fig. 4. Simulated variation of cladding refractive index effective value vs incident light wavelength.

In Fig. 5 there are presented the variations of phase matching curves. There are presented results simulated for the investigated LPGFS for the first ten cladding propagation modes simulated for the investigating LPGFS.

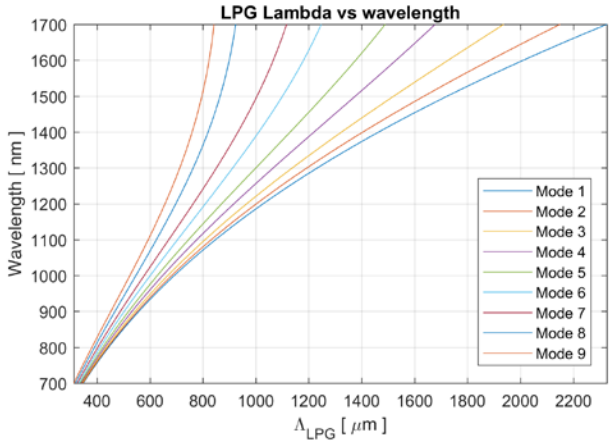

Fig. 5. The phase matching curves with wavelength and with long period grating period length, Λ_{LPG}, calculated for the first nine cladding modes.

The following procedure is quite simple: imagine a horizontal or vertical line, i.e. corresponding to a given value of Λ_{LPG} or light wavelength; the intersection points of this horizontal or vertical line with the phase matching curves defines the peaks λ_{res} of absorption bands appearing the optical fiber transmission spectrum. In common cases, for a given Λ_{LPG}, at a wavelength of the emission spectrum of a light source coupled to the LPGFS, corresponds several absorption bands each of them being induced by energy transfer to a cladding propagation mode.

In Figs. 6 - 12 there are presented the simulations made starting from the temperature of 0 ºC and jumps of 50 ºC, 60 ºC, 70 ºC, 80 ºC, 90 ºC, 100 ºC and 150 ºC. The initial absorption band has the peak located at 980.55 nm and a bandwidth of 21.76 nm. In each of these graphs the initial absorption band simulated at 0 ºC is represented in blue, while the final (shifted) absorption band is represented in red (dashed).

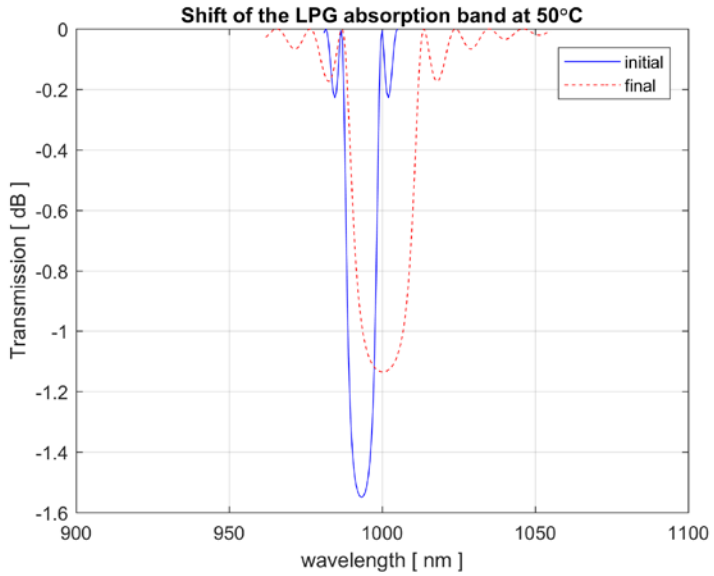

Fig. 6. The spectral shift of the 980.55 nm absorption band peak to 1000.12 nm wavelength under the effect of a relative temperature variation of 50 ºC.

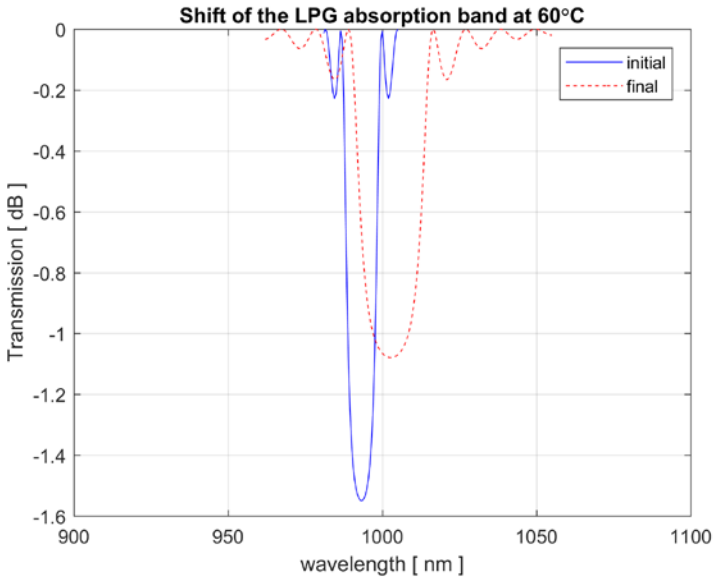

Fig. 7. The spectral shift of the 980.55 nm absorption band peak to 1002.75 nm wavelength under the effect of a relative temperature variation of 60 ºC.

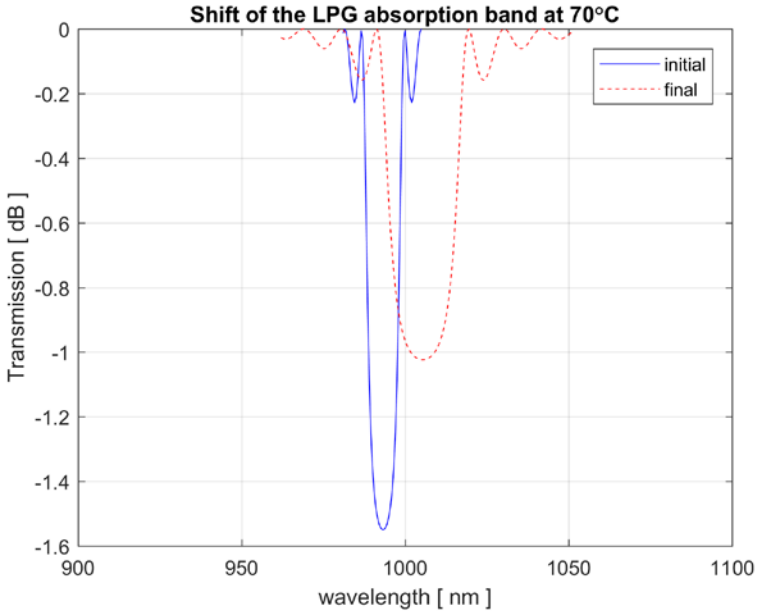

Fig. 8. The spectral shift of the 980.55 nm absorption band peak to 1005.12 nm wavelength under the effect of a relative temperature variation of 70º C.

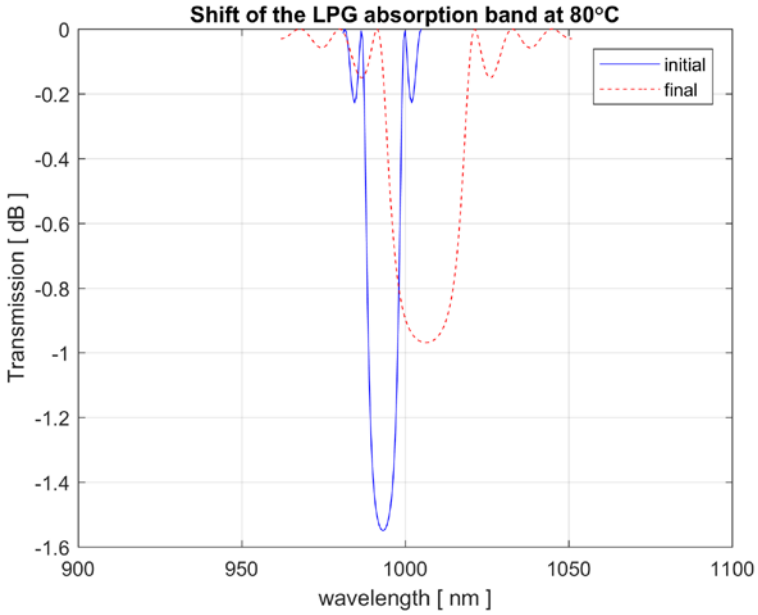

Fig. 9. The spectral shift of the 980.55 nm absorption band peak to 1006.52 nm wavelength under the effect of a relative temperature variation of 80º C.

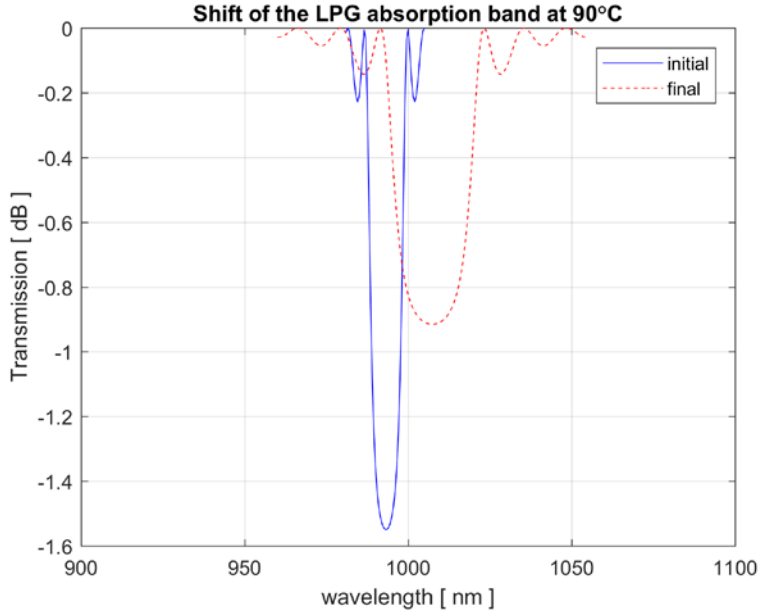

Fig. 10. The spectral shift of the 980.55 nm absorption band peak to 1007.25 nm wavelength under the effect of a relative temperature variation of 90º C.

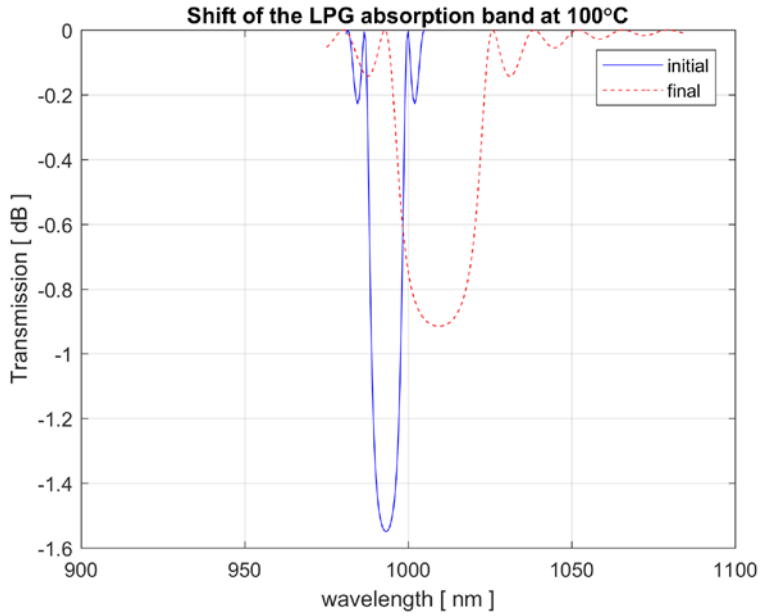

Fig. 11. The spectral shift of the 980.55 nm absorption band peak to 1009.19 nm wavelength under the effect of a relative temperature variation of 100º C.

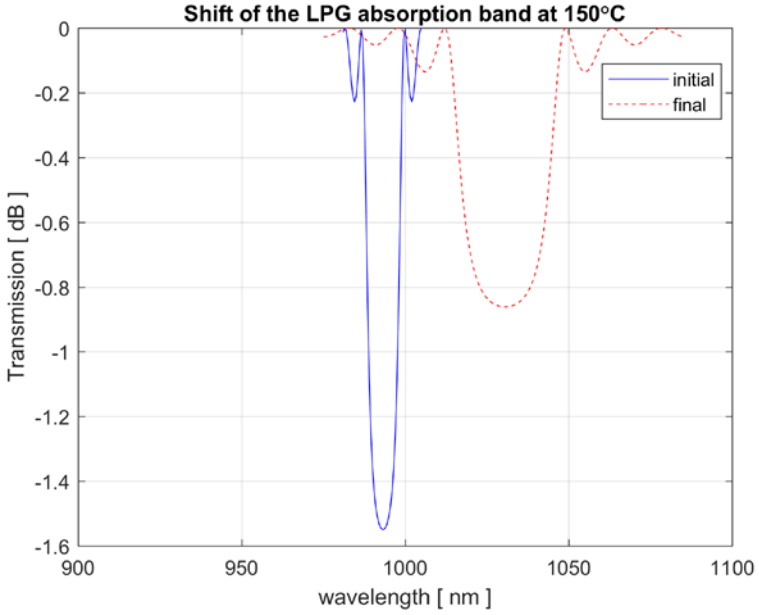

Fig. 12. The spectral shift of the 980.55 nm absorption band peak to 1030.07 nm wavelength under the effect of a relative temperature variation of 150º C.

There are presented the simulation results at 50 ºC temperature consisting in shifting the initial absorption band at 1000.12 nm and broadening at 40.55 nm (Fig. 6), at 60 ºC temperature consisting in shifting the initial absorption band at 1002.75 nm and broadening at 41.67 nm (Fig. 7), at 70 ºC temperature consisting in shifting the initial absorption band at 1005.12 nm and broadening at 42.45 nm (Fig. 8), at 80 ºC temperature consisting in shifting the initial absorption band at 1006.52 nm and broadening at 44.82 nm (Fig. 9), at 90 ºC temperature consisting in shifting the initial absorption band at 1007.25 nm and broadening at 47.57 nm (Fig. 10), at 100 ºC temperature consisting in shifting the initial absorption band at 1009.19 nm and broadening at 49.65 nm (Fig. 11) and at 150 ºC temperature jump consisting in shifting the initial absorption band at 1021.25 nm and broadening at 55.25 nm (Fig. 12).

Summarizing the simulation results presented in Figs. 6 - 12, it is worth to notice that the spectral shift of the initial absorption band at 0 ºC to the values of peak wavelength corresponding to the temperatures of 50 ºC, 60 ºC, 70 ºC, 80 ºC, 90 ºC, 100 ºC and 150 ºC has a relatively linear increase or fitted with a slow parabolic curve which cannot be synthetized by a rigorously deduced analytical relation (see Table 1).

Table 1

Linearity of the spectral shift

Temperature	Spectral shift [nm]	Linear trend [nm]
50 °C	19.57	17.82
60 °C	22.20	20.72
70 °C	24.57	23.61
80 °C	25.97	26.51
90 °C	26.70	29.40
100 °C	28.64	32.30
150 °C	49.52	46.77

As expected, the simulations of the initial absorption band located at 980.55 nm and having a bandwidth of 21.76 nm spectral shifts and broadenings induced by damages of polymer matrix situated at different distances from the optical fiber. The variations of n_{effco} and n_{clad}^{i} on bending radius of curvature and, consequently, of λ^{i}, can be simulated only numerically using very few analytical relations like Eq. (6).

Also, the broadening of the initial absorption band increase approximately linear in the same range of temperatures (see Table 2). The initial absorption band broadening variation versus temperature cannot be defined analytically by a rigorously deduced mathematical relation.

Table 2

Linearity of the bandwidth broadening

Temperature	Bandwidth broadening [nm]	Linear trend [nm]
50 °C	18.79	18.68
60 °C	19.91	20.23
70 °C	20.69	21.79
80 °C	23.06	23.34
90 °C	25.81	24.90
100 °C	27.89	26.45
150 °C	33.49	34.23

4. Conclusions

For development of a software package dedicated for the measurement of automobile composite material parts temperature, an optical LPGFS manufactured in a given commercial optical fiber and embedded into different types of polymers used as matrix for composite materials was simulated in order to improve its

design. Aiming to this purpose, the results obtained in calculations of core and clad effective refractive indexes variations over an extended guided light propagation wavelength range were obtained and used as a starting point of the composite properties simulation process. On this basis, for a given LPG period, there were calculated resonance wavelengths characteristics for several clad propagation modes, a number which can be extended. The results obtained in calculation of coupling coefficients of core and clad radiation modes, followed by the ones obtained in evaluation of absorption coefficients are presented as the simulation next stages. As the final two stages, the transmission spectra, the shift and the bandwidth broadening specific for a resonant wavelength, both induced by a bending deformation of optic fiber, are presented as calculated by using the developed software design package. The simulation results are in good agreement with experimental ones obtained from literature. In subsidiary, the presented results are part of a software design package dedicated to optimization of long period grating parameters, overall length and period, which are to be manufactured into a given single mode fiber, with the environment parameters to be measured with the resulting fiber optic sensor. In this sense, the software design package proves to be useful for calculation of core and clad refractive indexes variations with propagation wavelength, long period grating resonance wavelengths as depending on its period, the absorption coefficients at these resonance wavelengths and consequently, of its transmission spectra. The above mentioned long period grating software design package is under current development, the immediate improvement will consist in using the three layers optic fiber model and in increasing the number of cladding propagation modes used in calculations.

This research is supported by MANUNET grant MNET17/ NMCS0042 and by the Core Program project no. PN 18 28.01.01.

R E F E R E N C E S

[1]. *B. A. Childers, M. E. Froggatt, S. G. Allison, T. C. Moore, D. A. Hare, et al.*, "Use of 3000 Bragg grating strain sensors distributed on four eight-meter optical fibers during static load tests of a composite structure", in Proc SPIE, **vol. 4332**, pp. 133–142, 2001.

[2]. *J. R. Dunphy, G. Meltz, F. Lamm, W. Morey*, "Multi-function, distributed optical fiber sensor for composite cure and response monitoring", in Proc SPIE, **vol. 1370**, pp. 116–118, 1990.

[3]. *Y. H. Shen, W. Zhao, T. Sun, K.T.V. Grattan*, "Characterization of optical fibre thermometer using Tm3+:YAG crystal, based on fluorescence lifetime approach", in Sensor Actuat A-Phys, **vol. 109,** pp. 53-59, 2003.

[4]. *S. Pal, J. Mandal, T. Sun, K.T.V. Grattan*, "Analysis of thermal decay and prediction of operational lifetime for a type I boron-germanium codoped Fiber Bragg grating", in Appl Optics, **vol. 42,** pp. 2188-2197, 2003.

[5]. *L. Ren, H. N. Li, J. Zhou, D. S. Li, L. Sun*, "Health monitoring system for offshore platform with fiber Bragg grating sensors", in Opt Eng, **vol. 45,** no. 8**,** pp. 1-9, 2006.

[6]. *Y. J. Rao, B. Hurle, D. J. Webb, D. A. Jackson, L. Zhang, I. Bennion*, "In-situ temperature monitoring in NMR machines with a prototype in-fiber Bragg grating sensor system", in Procs OFS12, Williamsburg, VA, USA, 1997, pp. 646-649.

[7]. *E. J. Friebele*, "Fiber Bragg grating strain sensor: Present and future applications in smart structures", in Opt Photonics, vol. 9, no. 8, 1998, pp. 33-37.

[8]. *Y. J. Rao, D. J. Webb, D. A. Jackson, L. Zhang, I. Bennion*, "In-fibre Bragg grating temperature sensor system for medical applications", in J Lightwave Technol, **vol. 15**, no. 5, 1997, pp. 779-785.

[9]. *E. Samset, T. Mala, R. Ellingsen, I. Gladhaug, O. Søreide, E. Fosse*, "Temperature measurement in soft tissue using a distributed fibre Bragg-grating sensor system", in Minim Invasiv Ther, **vol. 10**, 2001, pp. 89-93.

[10]. *A. Othonos*, "Fiber Bragg gratings", in Rev Sci Instrum, **vol. 68**, no. 12, Sep. 1997, pp. 4309-4341.

[11]. *D. Savastru, S. Miclos, R. Savastru, I. Lancranjan*, "Numerical Analysis of a Smart Composite Material Mechanical Component Using an Embedded Long Period Grating Fiber Sensor", in Proc SPIE, **vol. 9517**, 95172A, 2015.

[12]. *S. Miclos, D. Savastru, R. Savastru, I. Lancranjan*, "Numerical analysis of Long Period Grating Fibre Sensor operational characteristics as embedded in polymer", in Compos Struct, vol. **183**, no. SI, 2018, pp. 521-526.

[13]. *D. Savastru, S. Miclos, R. Savastru, I. Lancranjan*, "Study of thermo-mechanical characteristics of polymer composite materials with embedded optical fibre", in Compos Struct, vol. **183**, no. SI, 2018, pp. 682-687.

[14]. *A. Othonos, K. Kalli*, Fiber Bragg Gratings: Fundamentals and Applications in Telecommunication and sensing, Artech House, Boston, 1999.

[15]. *Y. J. Rao*, "Recent progress in applications of in-fibre Bragg grating sensors", in Opt Laser Eng, **vol. 31**, no. 4, Apr. 1999, pp. 297-324.

[16]. *A. D. Kersey, M. A. Davis, H. J. Patrick, M. LeBlanc, K. P. Koo, et al.*, "Fiber Grating Sensors", in J Lightwave Technol, **vol. 15**, no. 8, 1997, pp. 1442-1463.

[17]. *V. Mizrahi, T. Erdogan, D. J. DiGiovanni, P. J. Lemaire, et al.*, "Four channel fiber grating demultiplexer", in Electron Let, **vol. 30**, no. 10, 1994, pp. 780-781.

[18]. *S. Miclos, D. Savastru, I. Lancranjan*, "Numerical Simulation of a Fiber Laser Bending Sensitivity", in Rom Rep Phys, **vol. 62**, no. 3, 2010, pp. 519-527.

[19]. *I. Lancranjan, S. Miclos, D. Savastru*, "Numerical simulation of a DFB-fiber laser sensor (I)", in J Optoelectron Adv M, **vol. 12**, no. 8, Aug. 2010, pp. 1636-1645.

[20]. *I. Lancranjan, S. Miclos, D. Savastru, A. Popescu*, "Numerical simulation of a DFB-fiber laser sensor (II) - theoretical analysis of an acoustic sensor", in J Optoelectron Adv M, **vol. 12**, no. 12, Dec. 2010, pp. 2456-2461.

[21]. *R. Savastru, I. Lancranjan, D. Savastru, S. Miclos*, "Numerical simulation of distributed feed-back fiber laser sensors", in Proc SPIE, **vol. 8882**, 88820Y, 2013.

[22]. *S. Miclos, D. Savastru, R. Savastru, I. Lancranjan*, "Design of a Smart Superstructure FBG Torsion Sensor", in Proc SPIE, vol. **9517**, 95172B, 2015.

[23]. *D. Savastru, S. Miclos, R. Savastru, I. Lancranjan*, "Analysis of optical microfiber thermal processes", in Rom Rep Phys, **vol. 67**, no. 4, 2015, pp. 1586-1596.